

See discussions, stats, and author profiles for this publication at: <https://www.researchgate.net/publication/312411625>

Application of Observability Analysis to Space Object Tracking

Conference Paper · January 2017

DOI: 10.2514/6.2017-1258

CITATIONS

5

READS

239

3 authors, including:



John Crassidis

University at Buffalo, The State University of New York

258 PUBLICATIONS 10,093 CITATIONS

SEE PROFILE

Application of Observability Analysis to Space Object Tracking

Andrew D. Dianetti*

University at Buffalo, State University of New York, Amherst, New York, 14260-4400

Ryan Weisman†

Air Force Research Laboratory, Kirtland Air Force Base, New Mexico 87117

John L. Crassidis‡

University at Buffalo, State University of New York, Amherst, New York, 14260-4400

An information-driven estimator is developed to allow for more accurate estimation of the orbit and appropriate parameters such as area-to-mass ratio and attitude, of a space object. From the information dilution theorem, when additional states are added to a filter with the number of observations held constant, the uncertainty in each state will increase. Likewise, failure to compensate for uncertainty in system states and/or parameters requires process noise compensation which increases the uncertainty of the estimate. The system observability can be used to determine when enough information exists to estimate additional states and which states can be appropriately estimated at that time. Tracking examples of space objects in multiple orbit regimes from angles-only data are presented, examining the estimation accuracy and uncertainty for orbit and orbit with area-to-mass ratio. Light curve measurements of a faceted vehicle are added, and estimation of orbit and attitude is considered. It is shown that the proposed adaptive approach based on the observability and assessment of measurement information content performs better over the entire time period than a single filter with a constant number of states.

I. Introduction

There exists an ever-increasing need to characterize space objects for accurate prediction of motion. This is the foundation of space situational awareness. To characterize these objects, filtering techniques are used to estimate object parameters. The most commonly estimated states are the object's orbit, which is the most basic, yet most important attribute to estimate as it tells where the object is and where it is going – information that is paramount to accurate knowledge of the space population and its evolution. Due to orbital perturbations, the orbital states alone do not provide an accurate prediction of the object's position. Additional attributes, such as ballistic coefficient or Area-to-Mass Ratio (AMR), or attitude state and object shape, can provide a more complete picture of the object and allow for more accurate orbit propagation. Traditionally, in the tracking of space objects, the six orbital states plus a ballistic coefficient are estimated [1]. However, the ballistic coefficient has limitations in that it uses a "cannonball model" which assumes the object is spherical, possessing constant AMR and reflectivity properties. This is seldom the case, and the effects of orbital perturbations, such as Solar Radiation Pressure (SRP), can be more accurately modeled through methods which account for the object's shape, attitude, and reflectivity properties [2].

If light curve data, the time history of an object's measured reflectance, is available, it has been shown that attitude observability can exist [3]. Shape estimation has been demonstrated using light curve data [4],

*Graduate Student, Department of Mechanical & Aerospace Engineering. Email: andrewdi@buffalo.edu. Student Member AIAA.

†Research Aerospace Engineer, Space Vehicles Directorate.

‡CUBRC Professor in Space Situational Awareness, Department of Mechanical & Aerospace Engineering. Email: johncc@buffalo.edu. Fellow AIAA.

as has attitude estimation [5]. These efforts have been extended to estimation of shape, attitude, and surface parameters [6] and simultaneous position, velocity, attitude, angular rate, and surface parameter estimation [7]. However, with a limited amount of data, the more attributes that are included in the state vector, the larger the uncertainties in each state become. This is explained by the Information Dilution Theorem [8] with the caution noted in [7]. By estimating additional attributes, it is possible that uncertainty in the orbital state may increase, contrary to the purpose of these efforts. In cases where the estimated state uncertainty is of the same order of magnitude or larger than the estimate itself, it is logical to conclude that the estimate is not particularly useful. This indicates that the available information is not being used in the most appropriate manner.

This work assesses the observability of the system to allow the choice of estimated states to be chosen more rigorously. The observability of different parameters, such as AMR and attitude states is analyzed, and conditions are determined to indicate when it is appropriate to begin additional parameter estimation. A consider (Schmidt-Kalman) filter is constructed to estimate the states; this allows parameters to be added and removed from the state vector while maintaining correlation information. The inclusion of additional states is automatically triggered based upon measurement information and observability assessment. This paper will give a condensed overview the work presented in Ref. [9], and also presents a method that employs both information analysis and Multiple-Model Adaptive Estimation (MMAE) to allow for changing the choice of estimated states when such states are not independent of each other (and the Schmidt-Kalman formulation will thus not work).

The paper is structured as follows. First, the system model is described, including the orbit and attitude dynamics models and the measurement models. Then, different measures of observability are discussed as they relate to the observability Gramian and information matrix. An overview of the filtering process is discussed, including definition of the orbit and attitude states, the implementation of consider filtering, and use of multiple model adaptive estimation. Results of the cases of angles-only measurements, and angles and light curve measurements are presented. The performance of filters that consider different choices of state variables, as well as adaptive filters based on observability, is presented.

II. Orbit and Attitude Model

A. Orbit and Attitude Dynamics Model

An object's orbit can be represented in many different frameworks, such as a concurrent position and velocity vector, Classical (Kepler) Orbital Elements, Equinoctial Elements, and Modified Equinoctial Elements. In this section, the orbital dynamics are described in the Cartesian Earth-Centered Inertial (ECI) framework, although the subsequent filtering has been performed using both this framework and a set of Modified Equinoctial Elements, which are a set of curvilinear elements that do not suffer from singularities [10].

In the Cartesian ECI framework, the orbital dynamics model can be written as [11]

$$\ddot{\mathbf{r}} = -\frac{\mu}{\|\mathbf{r}\|^3} + \mathbf{a}_d \quad (1)$$

where \mathbf{r} is the position vector, μ is the standard gravitational parameter, and \mathbf{a}_d contains all accelerations due to perturbations, which have the general form

$$\mathbf{a}_d = \mathbf{f}(\mathbf{r}, \dot{\mathbf{r}}, \mathbf{q}, \boldsymbol{\omega}, \mathbf{p}) \quad (2)$$

where \mathbf{q} is the quaternion which represents the attitude, $\boldsymbol{\omega}$ is the angular rate, and \mathbf{p} contains any spacecraft parameters, such as shape and dimensions, mass, inertia, and surface reflectances. These perturbations are due to many sources, including the zonal effects from the non-spherical Earth, acceleration due to other bodies such as the moon and Sun, drag, and SRP [12]. Analytic equations for these effects are given in [11]. Forces such as drag, SRP, and gravity gradient couple the attitude and orbital dynamics. The acceleration due to drag is given in the Earth-Centered Earth-Fixed (ECEF) frame

$$\mathbf{a}_{\text{drag}}^{\text{ECEF}} = -\frac{1}{2}C_d \left(\frac{A_{\text{proj}}}{m} \right) D \|\dot{\mathbf{r}}^{\text{ECEF}}\| \dot{\mathbf{r}}^{\text{ECEF}} \quad (3)$$

where C_d is the drag coefficient, D is the density of the atmosphere, and $\dot{\mathbf{r}}^{\text{ECEF}}$ is the velocity in the ECEF frame, which rotates with the earth. The drag vector can then be rotated into the inertial (ECI) frame

through

$$\mathbf{a}_{\text{drag}}^I = A_{\text{ECEF}}^T \mathbf{a}_{\text{drag}}^{\text{ECEF}} \quad (4)$$

where A_{ECEF} is the rotation from the ECI to the ECEF frame.

While drag is negligible for objects in Geostationary Orbit (GEO), the effects of SRP are significant. The acceleration due to SRP is given by [11]

$$\mathbf{a}_{\text{SRP}} = - \left(\frac{\Phi_{\text{SR}}}{c} \right) \left(\frac{A_{\text{proj}}}{m} \right) C_R \mathbf{u}_{\text{sun}}^B \quad (5)$$

where Φ_{SR} is the solar flux, $c = 299,792,458$ m/s is the speed of light in a vacuum, C_R is coefficient of reflectivity, m is the mass, and $\mathbf{u}_{\text{sun}}^B$ is the Sun unit vector expressed in the body frame. For SRP, the projected area is along the direction of $\mathbf{u}_{\text{sun}}^B$, and for drag, the projected area is along the direction of $\dot{\mathbf{r}}^{\text{ECEF}}$. If the object can be represented as a collection of N facets, then

$$A_{\text{proj}} = \sum_{i=1}^N A_i \Theta_i \quad (6)$$

where

$$\Theta_i = \begin{cases} \cos \theta_i, & \text{if } \theta_i \leq \pi \\ 0, & \text{if } \theta_i > \pi \end{cases} \quad (7)$$

and θ_i is the angle between the facet unit normal vector and the object-to-Sun unit vector for SRP, and velocity direction for drag. Each facet has a constant unit vector in the body frame, $\mathbf{u}_{n,i}^B$, which can be rotated to the inertial frame by

$$\mathbf{u}_{n,i}^I = A^T(\mathbf{q}) \mathbf{u}_{n,i}^B \quad (8)$$

Then, the angle θ_i is given by

$$\cos \theta_i = (A^T(\mathbf{q}) \mathbf{u}_{n,i}^B) \cdot \mathbf{u}_{\text{proj}}^I \quad (9)$$

where $\mathbf{u}_{\text{proj}}^I = \mathbf{u}_{\text{sun}}^I$ for SRP and $\mathbf{u}_{\text{proj}}^I = \mathbf{u}_{\text{vel}}^I$ for drag, where $\mathbf{u}_{\text{vel}}^I$ is the direction of the velocity in the ECI frame, and can be determined by

$$\mathbf{u}_{\text{vel}}^{\text{ECEF}} = \frac{\dot{\mathbf{r}}^{\text{ECEF}}}{\|\dot{\mathbf{r}}^{\text{ECEF}}\|} \quad (10a)$$

$$\mathbf{u}_{\text{vel}}^I = A_{\text{ECEF}}^T \mathbf{u}_{\text{vel}}^{\text{ECEF}} \quad (10b)$$

The relation between $\mathbf{u}_{\text{sun}}^I$ and $\mathbf{u}_{\text{sun}}^B$ is given by $\mathbf{u}_{\text{sun}}^I = A^T(\mathbf{q}) \mathbf{u}_{\text{sun}}^B$. The attitude matrix A and the quaternion \mathbf{q} are simply different realizations of the same rotation and the attitude matrix can be determined from the quaternion through [13]

$$A(\mathbf{q}) = \Xi^T(\mathbf{q}) \Psi(\mathbf{q}) \quad (11)$$

with

$$\Xi(\mathbf{q}) = \begin{bmatrix} q_4 I_{3 \times 3} + [\boldsymbol{\varrho} \times] \\ -\boldsymbol{\varrho}^T \end{bmatrix} \quad (12a)$$

$$\Psi(\mathbf{q}) = \begin{bmatrix} q_4 I_{3 \times 3} - [\boldsymbol{\varrho} \times] \\ -\boldsymbol{\varrho}^T \end{bmatrix} \quad (12b)$$

where $I_{3 \times 3}$ is a 3×3 identity matrix, and $[\boldsymbol{\varrho} \times]$ is the standard cross-product matrix. The quantities q_4 and $\boldsymbol{\varrho}$ are the elements of the quaternion:

$$\mathbf{q} = \begin{bmatrix} \boldsymbol{\varrho} \\ q_4 \end{bmatrix} \quad (13)$$

The quaternion kinematics is given by the equation [13]

$$\dot{\mathbf{q}} = \frac{1}{2} \Xi(\mathbf{q}) \boldsymbol{\omega} = \frac{1}{2} \Omega(\boldsymbol{\omega}) \mathbf{q} \quad (14)$$

where

$$\Omega(\boldsymbol{\omega}) = \begin{bmatrix} -[\boldsymbol{\omega} \times] & \boldsymbol{\omega} \\ -\boldsymbol{\omega}^T & 0 \end{bmatrix} \quad (15)$$

and in the absence of control torques

$$\dot{\boldsymbol{\omega}} = \boldsymbol{\alpha}_d \quad (16)$$

or all angular acceleration is due to disturbance torques. It is evident that there is a coupling between the orbital and attitude dynamics through the A_{proj} term, which is a function of the object's attitude and its position in orbit.

B. Measurement Model

Available measurements for orbit state estimation typically include a set of angle measurements, and sometimes for LEO objects, the range from the observer. Angle measurements are taken to be topocentric right ascension and declination. If attitude state is to be estimated, additional measurements must be taken; typically, brightness measurements. The measurement model is given by

$$\mathbf{y} = \mathbf{h}(\mathbf{x}) + \boldsymbol{\nu} \quad (17)$$

where \mathbf{y} are the output measurements, \mathbf{x} are the states, and $\boldsymbol{\nu}$ is the measurement noise, which is zero-mean Gaussian noises process with covariance R , and

$$\mathbf{h}(\mathbf{x}) = \begin{bmatrix} \alpha \\ \delta \end{bmatrix} \quad (18)$$

for the angles-only case, where α is right ascension and δ is declination. If light curve data is available, the measurements can be written as

$$\mathbf{h}(\mathbf{x}) = \begin{bmatrix} \alpha \\ \delta \\ m_{\text{app}} \end{bmatrix} \quad (19)$$

where m_{app} is apparent magnitude. If the slant range ρ is available, it can also be included in $\mathbf{h}(\mathbf{x})$. Here, the state vector \mathbf{x} includes the orbital states, such as the position and velocity vectors, as well as additional states such as AMR or attitude states.

The apparent magnitude, m_{app} , is computed using a Bidirectional Reflectance Distribution Function (BRDF) and assumed known shape model. The reflection model is explained in [3], and briefly summarized below. The reflection geometry is shown in Figure 1. Each facet has a set of three basis vectors (\mathbf{u}_n^B , \mathbf{u}_u^B , \mathbf{u}_v^B). The unit vector \mathbf{u}_n^B points in the direction of the outward normal to the facet, which is the same vector used

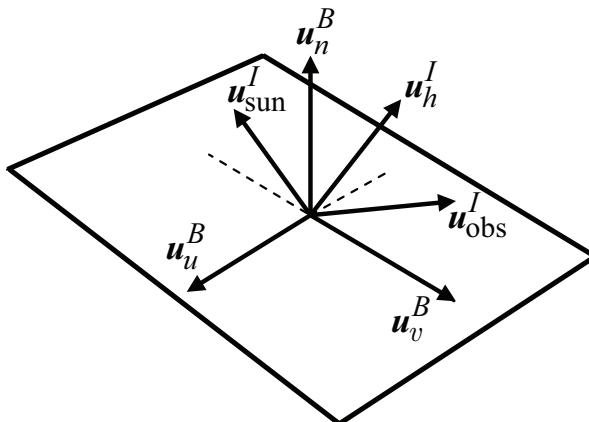


Figure 1. Reflection Geometry

in the SRP model, and the vectors \mathbf{u}_u^B and \mathbf{u}_v^B are in the plane of the facet. The object is assumed to be a rigid body so that the unit vectors \mathbf{u}_n^B , \mathbf{u}_u^B and \mathbf{u}_v^B do not change since they are expressed in the body frame. The vector \mathbf{u}_h^I is the normalized half vector between $\mathbf{u}_{\text{sun}}^I$ and the observation unit vector $\mathbf{u}_{\text{obs}}^I$. The observation vector is usually given in body coordinates with $\mathbf{u}_{\text{obs}}^B = A(\mathbf{q})\mathbf{u}_{\text{obs}}^I$.

The BRDF at any point on the surface is a function of two directions, the direction from which the light source originates and the direction from which the scattered light leaves the observed surface. The model in [14] decomposes the BRDF into a specular component and a diffuse component. The two terms sum to give the total BRDF:

$$\rho_{\text{total}, i} = \rho_{\text{spec}, i} + \rho_{\text{diff}, i} \quad (20)$$

The diffuse component represents light that is scattered equally in all directions (Lambertian) and the specular component represents light that is concentrated about some direction (mirror-like). Reference [14] develops a model for continuous arbitrary surfaces but simplifies for flat surfaces. This simplified model is employed in this work as shape models are considered to consist of a finite number of flat facets. Therefore the total observed brightness of an object becomes the sum of the contribution from each facet.

Under the flat facet assumption the specular term of the BRDF becomes

$$\rho_{\text{spec}, i} = \frac{\sqrt{(n_u + 1)(n_v + 1)}}{8\pi} \frac{(\mathbf{u}_{n, i}^I \cdot \mathbf{u}_h^I)^{n_u} (\mathbf{u}_h^I \cdot \mathbf{u}_{u, i}^I)^2 + n_v [1 - (\mathbf{u}_h^I \cdot \mathbf{u}_{v, i}^I)^2]}{\mathbf{u}_{n, i}^I \cdot \mathbf{u}_{\text{sun}}^I + \mathbf{u}_{n, i}^I \cdot \mathbf{u}_{\text{obs}}^I - (\mathbf{u}_{n, i}^I \cdot \mathbf{u}_{\text{sun}}^I)(\mathbf{u}_{n, i}^I \cdot \mathbf{u}_{\text{obs}}^I)} F_{\text{reflect}, i} \quad (21)$$

where the Fresnel reflectance is given by

$$F_{\text{reflect}, i} = R_{\text{spec}, i} + (1 - R_{\text{spec}, i}) (1 - \mathbf{u}_{\text{sun}}^I \cdot \mathbf{u}_{h, i}^I)^5 \quad (22)$$

The parameters of the Phong model that dictate the direction (locally horizontal or vertical) distribution of the specular terms are n_u and n_v . The diffuse term of the BRDF is

$$\rho_{\text{diff}, i} = \left(\frac{28R_{\text{diff}, i}}{23\pi} \right) (1 - R_{\text{spec}, i}) \left[1 - \left(1 - \frac{\mathbf{u}_n^I(i) \cdot \mathbf{u}_{\text{sun}}^I}{2} \right)^5 \right] \left[1 - \left(1 - \frac{\mathbf{u}_n^I(i) \cdot \mathbf{u}_{\text{obs}}^I}{2} \right)^5 \right] \quad (23)$$

The apparent magnitude of the object is the result of sunlight reflecting off of its surfaces along the line-of-sight to an observer. First, the fraction of visible sunlight that strikes an object (and not absorbed) is computed by

$$F_{\text{sun}, i} = C_{\text{sun,vis}} \rho_{\text{total}, i} (\mathbf{u}_{n, i}^I \cdot \mathbf{u}_{\text{sun}}^I) \quad (24)$$

where $C_{\text{sun,vis}} = 455 \text{ W/m}^2$ is the power per square meter impinging on a given object due to visible light striking the surface. If either the angle between the surface normal and the observer's direction or the angle between the surface normal and Sun direction is greater than $\pi/2$ then there is no light reflected toward the observer. If this is the case then the fraction of visible light is set to $F_{\text{sun}, i} = 0$.

The fraction of sunlight that strikes a surface that is reflected given by

$$F_{\text{obs}, i} = \frac{F_{\text{sun}, i} A_{\text{proj}, i} (\mathbf{u}_{n, i}^I \cdot \mathbf{u}_{\text{obs}}^I)}{d^2} \quad (25)$$

where d is the distance from the observer to the object. The reflected light is now used to compute the apparent brightness magnitude, which is measured by an observer through

$$m_{\text{app}} = -26.7 - 2.5 \log_{10} \left| \sum_{i=1}^N \frac{F_{\text{obs}, i}}{C_{\text{sun,vis}}} \right| \quad (26)$$

where -26.7 is the apparent magnitude of the Sun, and N is the total number of facets.

If position-level measurements are available, the six orbital states can be estimated, as well as the ballistic coefficient or AMR. This is observed as a change in the spacecraft's position due to the effect of SRP or drag. In this case, the object is modeled as a sphere, such that its AMR is independent of attitude, which is unknown. If light curve measurements are available, then attitude can also be estimated. Determining whether it is appropriate to employ a coupled orbit and attitude estimator or solely estimate orbit is one of the purposes of this effort.

III. Observability Measures

To assess the observability of system parameters and the amount of information contained in observations, there must be a means to quantify the observability. The information matrix can be defined as the inverse of the covariance matrix [15]

$$J_k = (P_k)^{-1} \quad (27)$$

where J_k is the information matrix at time t_k , and P is the covariance matrix. If the system is linearized at each time step, as in the Extended Kalman Filter (EKF) framework, the new information added from a single measurement at time t_{k+1} is given by

$$J_{\text{new},k+1} = H_{k+1}^T R_{k+1}^{-1} H_{k+1} \quad (28)$$

where

$$H = \frac{\partial h(\mathbf{x})}{\partial \mathbf{x}} \quad (29)$$

is the linearized matrix that maps states into measurements, and R_{k+1} is the measurement covariance matrix, typically constant for these observations. The total information available at time t_{k+1} is equal to the sum of the information from the previous k time steps and the new information given in Eq. (28). The information available from previous measurements can be mapped into the current state [15]

$$J_{k+1} = (Q_k + \Phi_k J_k^{-1} \Phi_k^T)^{-1} + H_{k+1}^T R_{k+1}^{-1} H_{k+1} \quad (30)$$

where Φ_k is the state transition matrix, used to map the system states forward through

$$\mathbf{x}_{k+1} = \Phi_k \mathbf{x}_k \quad (31)$$

The matrix Q_k is the process noise covariance, and Eq. (30) shows that a nonzero process noise contributes a loss of information compared to the case where there is no process noise. Using the definition of information from Eq. (27), Eq. (30) is identical to the covariance propagation and update of the EKF when the matrix inversion lemma is applied.

The information matrix over the entire time period $[0, T]$ can also be written in integral form as [16]

$$J = \int_0^T \Phi^T(t) H^T(t) R(t) H(t) \Phi(t) dt \quad (32)$$

If this is evaluated in discrete time, it becomes Eq. (30). This is closely related to the observability Gramian, which is defined as [15] [17]

$$W = \int_0^T \Phi^T(t) H^T(t) H(t) \Phi(t) dt \quad (33)$$

If the measurement covariance matrix is constant with time, as assumed in this work, then the information matrix and observability Gramian are directly related, and the information matrix thus provides a weighted assessment of observability. Other scalar measures of an observation contributing to reduction in uncertainty in state estimation can be considered, such as mutual information or entropy [18]. Mutual information is the reduction in uncertainty of the estimated states given additional measurements. Entropy is the amount of uncertainty left in the estimated states due to the additional measurements. If state observability is increased, this will result in an increased reduction of estimated state uncertainty, so focusing on observability and its corresponding matrix directly affect the mutual information scalar.

With the information matrix formed, a method is required to quantify the amount of information in the system, which is analogous to quantifying the observability. While verifying that the observability Gramian, or information matrix, is full rank will confirm that the system is observable, this does not assess the degree of observability. The determinant of the matrix is often used to assess the level of observability, however, such a measure does not provide information about the observability of individual states within the system. By taking a singular value decomposition, the observability of the modes of the system can be assessed. The magnitudes of the singular values will indicate the degree of observability of modes identified by the right-hand side vectors, which are composed of contributions from the system states. As such, it is possible to identify which states have stronger and weaker observability. As discussed by Krener and Ide [17]

and Hermann and Krener [19], Lie derivatives can be used as a measure of nonlinear system observability. The linearization of the object dynamics is avoided, but for evaluation of matrix rank, the measurement equations are still required to be linearized. Lie derivatives are convenient due to their recursive nature and can be implemented on a computer system. The same methods applied to the observability Gramian and information matrix to evaluate the singular values and their corresponding eigenvectors can be used. For a linearized system, the dynamic system model is

$$\mathbf{x}_{k+1} = \Phi_{k+1,k} \mathbf{x}_k + G_k \mathbf{w}_k \quad (34)$$

with the process noise $\mathbf{w}_k \sim N(0, Q_k)$, where Q_k is the process noise covariance. Entropy \mathbb{H} is defined as

$$\mathbb{H}(\hat{\mathbf{x}}) = \mathbb{E} \{-\ln p(\hat{\mathbf{x}})\} = - \int p(\hat{\mathbf{x}}) * \ln[p(\hat{\mathbf{x}})] dx = - \sum p(\hat{\mathbf{x}}_i) \ln(p(\hat{\mathbf{x}}_i)) \quad (35)$$

where p denotes a probability density function and \mathbb{E} denotes the expected value. Then, the mutual information $M(\mathbf{x}, \mathbf{y})$ is

$$M(\hat{\mathbf{x}}, \tilde{\mathbf{y}}) = \mathbb{E} \left\{ \ln \frac{p(\hat{\mathbf{x}}, \tilde{\mathbf{y}})}{p(\hat{\mathbf{x}})p(\tilde{\mathbf{y}})} \right\} \quad (36)$$

Then, since

$$p(\hat{\mathbf{x}}, \tilde{\mathbf{y}}) = p(\tilde{\mathbf{y}}|\hat{\mathbf{x}})p(\hat{\mathbf{x}}) = p(\hat{\mathbf{x}}|\tilde{\mathbf{y}})p(\tilde{\mathbf{y}}) \quad (37)$$

Eq. (36) becomes

$$M(\hat{\mathbf{x}}, \tilde{\mathbf{y}}) = \mathbb{E} \left\{ \ln \left(\frac{p(\tilde{\mathbf{y}}|\hat{\mathbf{x}})}{p(\tilde{\mathbf{y}})} \right) \right\} = \mathbb{H}\{\tilde{\mathbf{y}}\} - \mathbb{H}\{\tilde{\mathbf{y}}|\hat{\mathbf{x}}\} = \mathbb{H}\{\hat{\mathbf{x}}\} - \mathbb{H}\{\hat{\mathbf{x}}|\tilde{\mathbf{y}}\} \quad (38)$$

Now, assuming the process noise and measurement noise models are Gaussian, the probability density functions are [20]

$$p(\tilde{\mathbf{y}}|\hat{\mathbf{x}}) = \frac{1}{(2\pi)^{m/2}[\det(R)]^{1/2}} \exp \left\{ -\frac{1}{2} [\tilde{\mathbf{y}} - H\hat{\mathbf{x}}]^T R^{-1} [\tilde{\mathbf{y}} - H\hat{\mathbf{x}}] \right\} \quad (39a)$$

$$p(\hat{\mathbf{x}}) = \frac{1}{(2\pi)^{n/2}[\det(Q)]^{1/2}} \exp \left\{ -\frac{1}{2} [\hat{\mathbf{x}}_a - \hat{\mathbf{x}}]^T Q^{-1} [\hat{\mathbf{x}}_a - \hat{\mathbf{x}}] \right\} \quad (39b)$$

$$p(\tilde{\mathbf{y}}) = \frac{1}{(2\pi)^{m/2}[\det(D)]^{1/2}} \exp \left\{ -\frac{1}{2} [\tilde{\mathbf{y}} - H\hat{\mathbf{x}}_a]^T D^{-1} [\tilde{\mathbf{y}} - H\hat{\mathbf{x}}_a] \right\} \quad (39c)$$

where $D \equiv H^T Q H + R$ and $\hat{\mathbf{x}}_a$ denotes the *a priori* state estimate. Then, if Eqs. (39a)–(39c) and (17) are substituted into Eq. (38), the mutual information is

$$M(\mathbf{x}|\tilde{\mathbf{y}}) = \frac{1}{2} (\ln(\det(E)) - \ln(\det(R))) \quad (40)$$

where $E = HPH^T + R$.

Krener and Ide [17] define two metrics of observability. The first is referred to as the *local unobservability index* and is defined as the reciprocal of the smallest singular value. This measures how difficult it is to estimate the state from the output. The second is referred to as the *local estimation condition number* and is equal to the ratio of the smallest singular value to the largest singular value. These metrics can be extended to other singular values to assess the observability of each mode, where the contributions of each state to a particular mode is given by the right-hand eigenvectors.

IV. Information-Driven Filtering Process

A. State Definition and Consider Filtering

To improve the accuracy of the state estimates, it is desired to determine when there is sufficient information to begin estimating additional states. This is used to build an information-driven approach to estimating

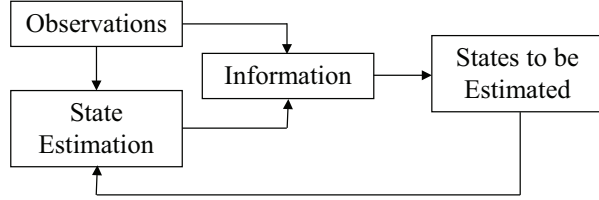


Figure 2. Concept of Information-Driven State Estimator

object states and parameters. Analysis of the available information in the system is used to determine the states to be estimated, and the filter is adapted to estimate these states based on the available information. This process is shown in Figure 2.

To accommodate the changing state dimensions through the filter, Consider Filtering (also known as Schmidt-Kalman Filtering) is used. In Consider Filtering, the system model depends on the estimated system states \mathbf{x} as well as parameters \mathbf{p} that are not estimated. If it is desired to reduce the dimension of the state vector, the removed states must be treated as parameters to preserve the correlation information with the other states. Simply eliminating states from the state vector and covariance matrix results in frequent divergence of the filter due to loss of this correlation information. The optimal augmented estimates are given by [20]

$$\begin{bmatrix} \hat{\mathbf{x}}_k^+ \\ \hat{\mathbf{p}}_k^+ \end{bmatrix} = \begin{bmatrix} \hat{\mathbf{x}}_k^- \\ \hat{\mathbf{p}}_k^- \end{bmatrix} + K_{z,k} \left(\tilde{\mathbf{y}}_k - \mathbf{h} \left(\begin{bmatrix} \hat{\mathbf{x}}_k^- \\ \hat{\mathbf{p}}_k^- \end{bmatrix} \right) \right) \quad (41)$$

where

$$K_{z,k} = \begin{bmatrix} K_k \\ 0 \end{bmatrix} \quad (42)$$

is the Kalman gain. Hence, it is seen that the parameters are not being estimated. The covariance matrix is partitioned into

$$P = \begin{bmatrix} P_{xx} & P_{xp} \\ P_{px} & P_{pp} \end{bmatrix} \quad (43)$$

where P_{xx} is the state covariance and is updated at each time step, while P_{pp} is the parameter covariance and remains constant. The matrix $P_{xp} = P_{px}^T$ contains the correlations between the updated state estimates and the parameters. Propagation and update equations for the covariance terms are given for the (linear) Kalman filter in [20] and are extended into the nonlinear case as an Extended Kalman Filter. An Unscented Consider Filter is presented in [21]. Both the EKF and Unscented Filters are implemented, and performance is found to be comparable. Unscented Filter results are presented in this paper.

The state vector $\hat{\mathbf{x}}_k$ contains, at minimum, the orbital states. The filtering results presented in this paper use the position and velocity vectors to define the orbit, although it has been verified that the filters also work using the Modified Equinoctial Elements [10]. Additional states, such as AMR and the attitude states, are switched between states $\hat{\mathbf{x}}_k$ and parameters $\hat{\mathbf{p}}_k$. Estimation of the additional states are “switched on” when it is determined that there is sufficient information to estimate them, otherwise, they are “switched off,” when they are not estimated, but correlations with the orbital state variables are preserved.

B. Attitude State Definition

Four parameters are required to provide a singularity-free attitude representation, however, these four parameters are subject to a constraint - in the case of the quaternion, the unit normal constraint. A multiplicative approach is used, where an error quaternion is estimated and multiplied with the prior quaternion estimate to provide the updated state estimate, where

$$\delta \mathbf{q} \equiv [\delta \boldsymbol{\varrho} \quad \delta q_4]^T \quad (44)$$

and the updated quaternion is given by

$$\hat{\mathbf{q}}_k^+ = \delta \mathbf{q}_k \otimes \hat{\mathbf{q}}_k^- \quad (45)$$

where quaternion multiplication using \otimes is defined in the same order as multiplying attitude matrices, as described in [22]. It is found that estimating $\delta\boldsymbol{\varrho}$ and then calculating δq_4 to satisfy the unit norm constraint does not work well with light curve measurements, as the value of $\delta\boldsymbol{\varrho}$ can have a magnitude greater than 1. However, the Generalized Rodrigues Parameters (GRP), as defined in [23], are found to work well. The GRPs are defined as

$$\delta\mathbf{p} \equiv f \frac{\delta\boldsymbol{\varrho}}{a + \delta q_4} \quad (46)$$

Here a is chosen to be 1, and $f = 2(a + 1)$, which gives $\delta\mathbf{p}$ components of roll, pitch, and yaw errors for small errors. Then Eq. (46) is inverted to give [24]

$$\delta q_4 = \frac{-a||\delta\mathbf{p}||^2 f \sqrt{f^2 + (1-a)^2 ||\delta\mathbf{p}||^2}}{f^2 + ||\delta\mathbf{p}||^2} \quad (47a)$$

$$\delta\boldsymbol{\varrho} = f^{-1}(a + \delta q_4)\delta\mathbf{p} \quad (47b)$$

C. Multiple-Model Adaptive Estimation

While the goal of this effort is to use the observability of the system parameters to intelligently choose which are to be estimated, MMAE provides an alternate approach in which an estimate can be determined from the results of a bank of filters that each estimate a different set of parameters. Here, the bank of filters is composed of a six-state orbit filter, a seven-state orbit and AMR filter, and optionally a twelve-state orbit and attitude filter. MMAE provides a state estimate by taking a weighted sum of the estimates from each filter, with weights determined by the likelihood of the state estimates conditioned on the measurement sequence. Parallel filters can be run that estimate different states, and the resulting state estimates and covariances from these filters can be combined into the weighted estimate for the orbit states. MMAE is assessed here to see if the estimates behave similarly to the information-driven filter estimates.

A derivation of the MMAE process can be found in [13]. Given the j^{th} probability density function $p(\tilde{\mathbf{y}}_k | \hat{\mathbf{x}}_k^{-(j)})$, the MMAE weights are computed as

$$w_k^{(j)} = w_{k-1}^{(j)} p(\tilde{\mathbf{y}}_k | \hat{\mathbf{x}}_k^{-(j)}) \quad (48)$$

which then must be normalized by

$$w_k^{(j)} \leftarrow \frac{w_k^{(j)}}{\sum_{j=1}^M w_k^{(j)}} \quad (49)$$

where \leftarrow denotes replacement, and M is the total number of filters used. Also, the weights give the probability of the j^{th} filter's contribution. Assuming the measurement model is Gaussian, the probability density function $p(\tilde{\mathbf{y}}_k | \hat{\mathbf{x}}_k^{-(j)})$ is given by

$$p(\tilde{\mathbf{y}}_k | \hat{\mathbf{x}}_k^{-(j)}) = \frac{1}{[\det(2\pi E_k^{-(j)})]^{1/2}} \exp \left\{ -\frac{1}{2} \mathbf{e}_k^{-(j)T} \left(E_k^{-(j)} \right)^{-1} \mathbf{e}_k^{-(j)} \right\} \quad (50)$$

where

$$\mathbf{e}_k^{-(j)} \equiv \tilde{\mathbf{y}}_k - \hat{\mathbf{y}}_k^{-(j)} \quad (51)$$

and, using the EKF convention,

$$E_k^{-(j)} = H_k^{(j)} P_k^{-(j)} H_k^{(j)T} + R_k^{(j)} \quad (52)$$

D. Transition from Cannonball to Faceted Model

The use of consider (Schmidt-Kalman) filtering to allow for a change in the estimated states has been discussed. This method is valid if the state vector is simply augmented, where new states are added. If this augmentation is carried out at an arbitrary time, the cross-correlation terms between the new state and existing states are typically assumed to be zero. This requires scaling up of the diagonal entries, which is the best that can be done in the absence of further information, but may result in slow convergence, or a “burn-in” time.

However, if the new states being added are not independent from the existing states - for example, if the area-to-mass ratio is replaced by the object's attitude states, simple augmentation of the state estimate and covariance cannot be performed. Since the attitude and area-to-mass ratio estimate are coupled, simply removing A/m as a state and replacing it with \mathbf{q} and $\boldsymbol{\omega}$ would involve removing information from the system. Furthermore, removing the cross-correlation terms at this time will often cause the filter to diverge.

To overcome these issues, a method which makes use of both information analysis and Multiple-Model Adaptive Estimation is presented. The MMAE process has been introduced in the prior section. MMAE requires running banks of filters, and thus increases computational requirements. As many objects may never gain enough information to warrant stepping to a faceted model, applying MMAE as a general technique to all objects is not advisable. An adaptive filter that makes use of both observability analysis and MMAE is presented to allow for increasing filter states without running MMAE at all times.

In this adaptive filter, the “cannonball” model is used until the rate of uncertainty in the area-to-mass ratio state falls below a certain threshold, indicating that the estimate is not becoming sufficiently better with the addition of new information. If, at this point, the uncertainty in this state is small compared to the state estimate itself, and the state estimate is also fluctuating substantially, then the cannonball model is deemed to be well-behaved, and estimation continues using this choice of states. However, if the uncertainty in area-to-mass ratio has not converged to a small value compared to the estimate magnitude, or the estimate experiences significant fluctuations, then it is concluded that the area-to-mass ratio is not capturing the dynamics well. In this case, the true area-to-mass ratio is likely changing due to changes in the spacecraft’s attitude. In this case, it may be worth using a faceted model with attitude estimation to more accurately capture the dynamics.

Angles, or angles and range, measurements alone do not provide sufficient information to estimate attitude. However, if visual magnitude (light curve) data is available, then attitude observability can exist [3]. The observability of attitude from light curve data is a function of the object’s shape, reflectivity parameters, and observation geometry. It is desired to use a faceted model and light curve data is available, then the mutual information of the state vector that includes the orbit and attitude is computed backward to the beginning of the observation track. If this mutual information is found to be significantly greater than the mutual information if light curve observations were not present, then it is determined that there exists sufficient observability of the attitude states to attempt including them. A similar analysis can be performed with other parameters of the faceted model, such as BRDF parameters, solar panel offset, etc, and these parameters could be included in the state vector if appropriate.

If it is determined that sufficient observability exists to attempt estimation of these parameters, a filter (using these parameters) is begun at the beginning of the current observation track. MMAE is then begun using a bank of this filter (or filters, if multiple parameter sets are evaluated) and the “cannonball” filter. If the weight of one filter becomes sufficiently close to 1 (in this case, taken to be greater than 0.99), then it is determined that said filter performs better for the system and contains the best-performing system model, and the other filters are switched off, ensuring that computational resources are not wasted. If the weight of the cannonball filter goes to 1, then it is concluded that even though attitude observability may exist, there exist other filters that preclude successful estimation of these parameters. If a faceted filter weight goes to 1, it is concluded that this model outperforms the cannonball model, and the cannonball filter is switched off. A diagram outlining this process is shown in Figure 3.

V. Results

Results for the angles-only and angles and lightcurves datasets are presented. Unscented filters are used to obtain the state estimates, and observability of the additional parameters is assessed. The models analyzed are summarized in Table 1.

A. Angles-Only Observations

First, the case of angles-only observations of right ascension and declination is investigated. With these measurements, it is possible to estimate the six orbit states and optionally the ballistic coefficient or area-to-mass ratio. The observability of the AMR state is assessed through the local estimation condition number [17], and this is considered in the choice of states.

The singular value decomposition of the information matrix is computed over time for the information

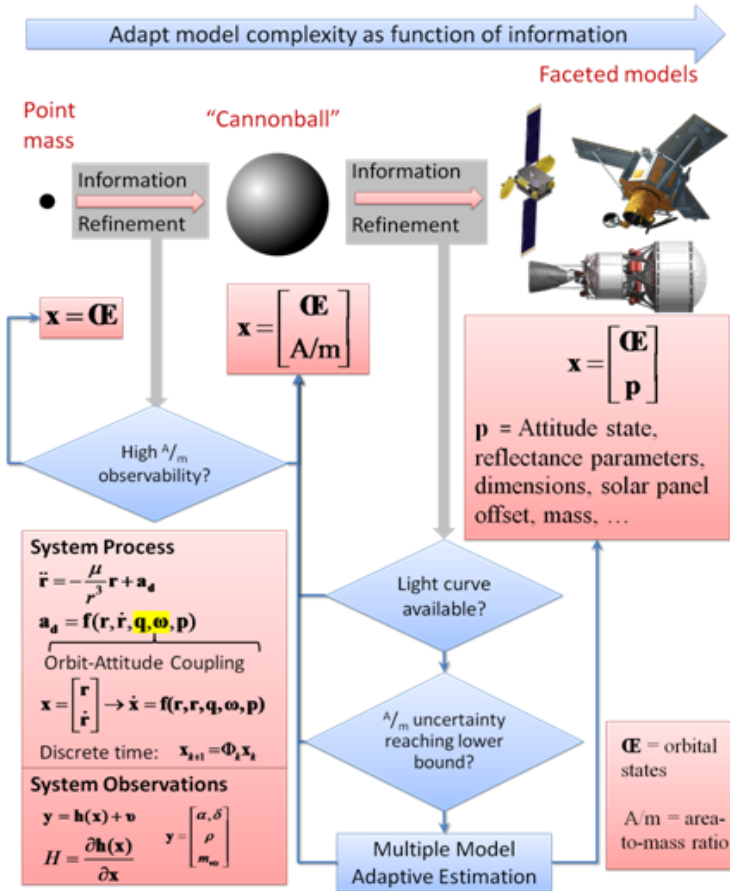


Figure 3. Information-Driven Adaptive Filtering Process

Table 1. Models Analyzed

Shape	AMR (m^2/kg)	Orbit	Observations	Obs. Cadence	Estimated States
Cannonball	0.0024	GEO	Angles Only	2 min	Orbit Orbit + AMR
Cannonball	0.4	GEO	Angles Only	2 min	Orbit Orbit + AMR
Cannonball	0.0024	GTO	Angles Only	30 sec	Orbit Orbit + AMR
Faceted	0.005-0.008	GEO	Angles Light Curve	2 min	Orbit Orbit + AMR Orbit + Attitude

matrix containing the six orbital states as well as the seven-state information matrix containing the AMR. The singular values are then normalized by the largest singular value to give the local estimation condition number [17]. It is found that there are six common modes that appear nearly identical in the two cases, and

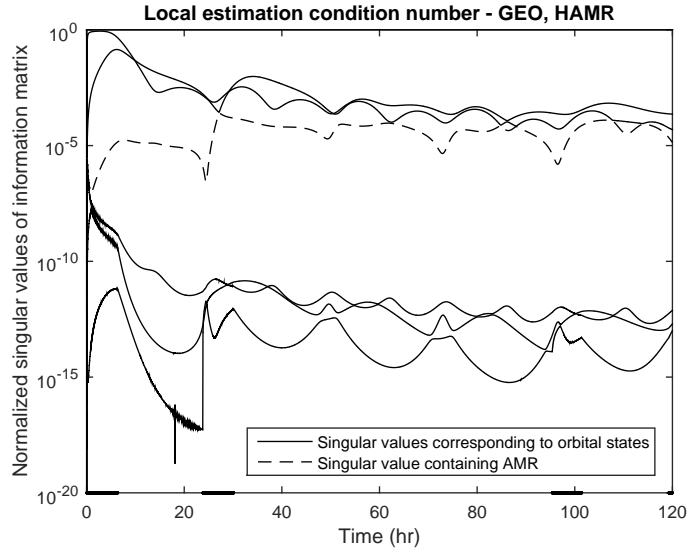


Figure 4. Normalized Singular Values of Information Matrix Showing Area-to-Mass Ratio Observability. Solid black line on x -axis indicates measurements available.

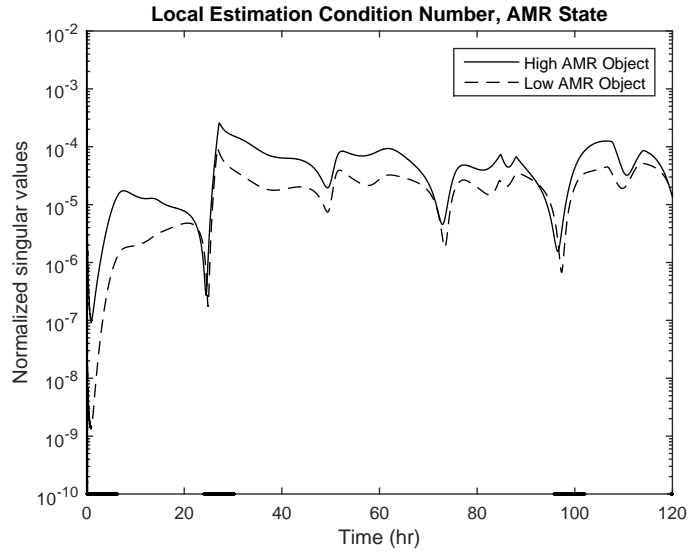


Figure 5. AMR Singular Value for High and Low AMR Objects. Solid black line on x -axis indicates measurements available.

an additional mode that contains the AMR in the seven-state case. These modes are shown for a low AMR object in Figure 4. The object truth data has been simulated using a cannonball model for this case, with an AMR of $0.0024 \text{ m}^2/\text{kg}$. Measurement noise of 1 arcsecond has been assumed. The observability of AMR is dependent on the AMR itself. For High Area-to-Mass Ratio (HAMR) objects, AMR has greater observability than for low AMR objects, as seen in Figure 5. This is explained by the fact that, as seen in Eq. (5), the greater influence of SRP causes larger changes to the orbit over a given time period, increasing observability. Figure 5 shows that a HAMR object ($\text{AMR} = 0.4$) has significantly greater observability during the first observation period, and although the difference becomes smaller as more nights of observation are added, it still maintains greater observability. An increase in observability is seen as a second night of observations is added. This shows the impact of assessing state observability on sensor tasking for information gain.

Using the observability of the mode containing AMR information, an adaptive filter is developed to

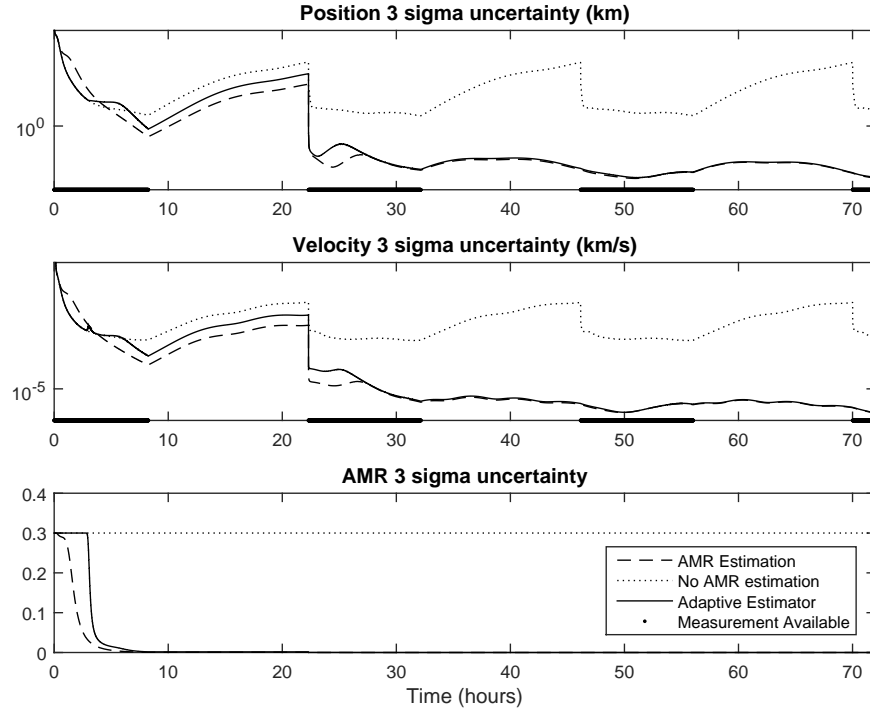


Figure 6. Uncertainty Bounds for Different Filters for Low AMR GEO Object

“switch on” AMR as an estimated state when sufficient information about that state is available. A value of 10^{-7} is chosen for the normalized singular value containing AMR information – once this value is reached, AMR gets added as a filter state. Figure 6 shows that initially, the orbit-only filter performs better – it has a lower uncertainty. After approximately three hours of observations, also with one observation taken every two minutes, the filter that estimates AMR begins to perform better and has a lower uncertainty. The adaptive (consider) filter initially follows the orbit-only filter, but then switches as the criteria is met, and has uncertainty bounds that approach the AMR filter. Thus, it is seen that this information-driven approach to selecting filtering states can provide a better estimate than filtering with a constant choice of states.

To demonstrate that this method is valid in other cases, a HAMR object is analyzed. The same filter is run, with the same switching criteria. As seen in Figure 7, the adaptive filter “switches on” AMR estimation much sooner, and begins to follow the uncertainty bounds of that filter more quickly, as the uncertainty rapidly decreases when estimating AMR. Additionally, the same low AMR object is simulated in a Geostationary Transfer Orbit (GTO), with observations taken near perigee. The singular value corresponding to the mode with AMR contributions is seen to behave similarly to the GEO cases, with similar magnitude, as shown in Figure 8. The greater observability, seen through the higher magnitude of this singular value indicates greater observability of AMR for objects closer to Earth. This is explained by the greater effect of AMR due to atmospheric drag, as opposed to just SRP for GEO objects. The criteria used in the GEO filters is found to work in this case as well. From these results and the equations of the physics and observations, it can be concluded that the observability of AMR impacts the performance of filters that use AMR as a state.

Multiple Model Adaptive Estimation is implemented for the angles-only case. The filter weights are shown in Figure 9. It is seen that initially, the filter that does not estimate AMR is given greater weight, indicating that the state estimates are better conditioned on the measurements. After approximately 1.25 hours, there is a sharp reversal, with the weight of the filter that favors AMR quickly increasing to 1. When compared with the uncertainty bounds in this case, it is seen that the filter weights begin to change when the bounds cross. Initially, the orbit-only filter has a lower uncertainty and is given a higher weight, but after some time the orbit and AMR filter has a lower uncertainty. It is at this point that the MMAE weights

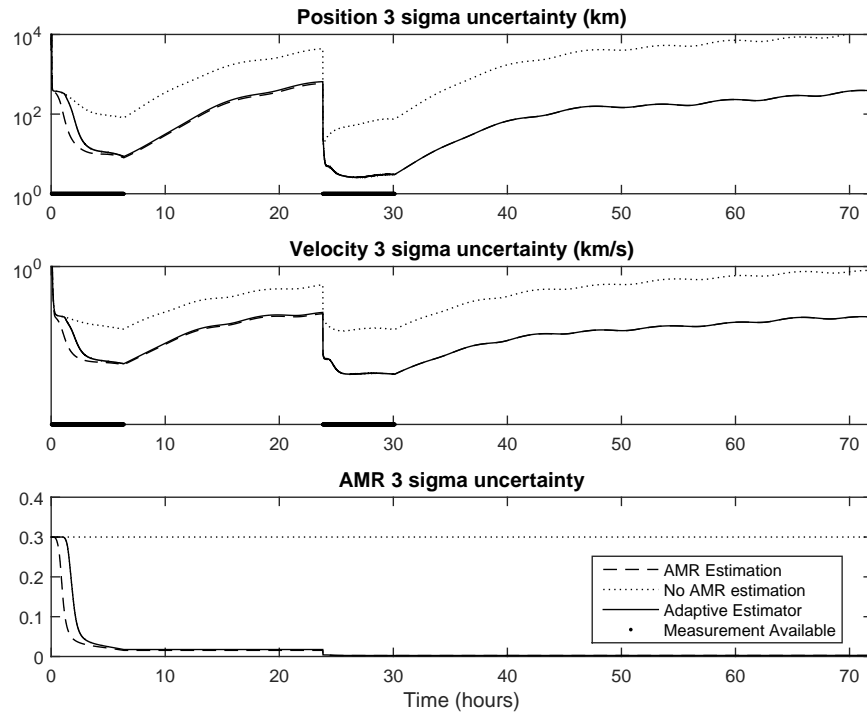


Figure 7. Uncertainty Bounds for Different Filters for HAMR GEO Object

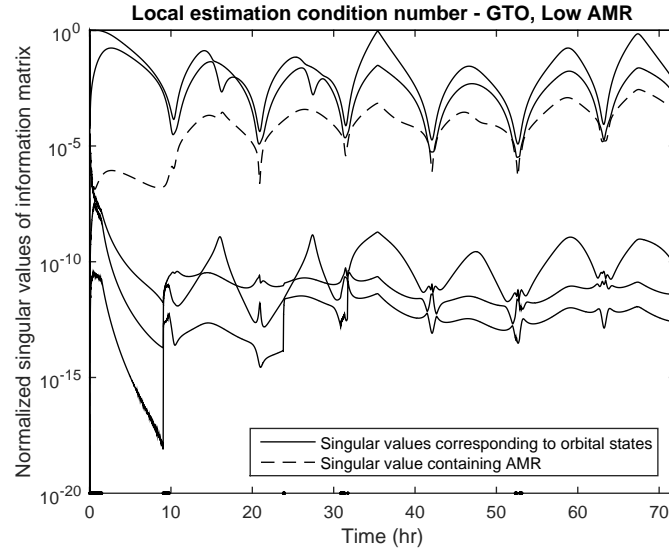


Figure 8. Normalized Singular Values of Information Matrix Showing ARM Observability for GTO Object with Observations Near Perigee. Solid black line on x -axis indicates measurements available.

cross. Since it has been shown that the uncertainty is driven by the observability, it is apparent that the MMAE behavior is also dependent on the observability.

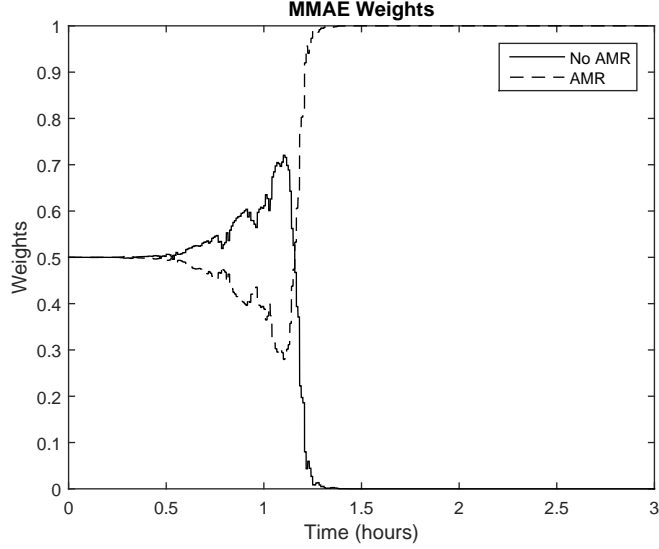


Figure 9. MMAE Weights for Orbit and Orbit + AMR Estimators.

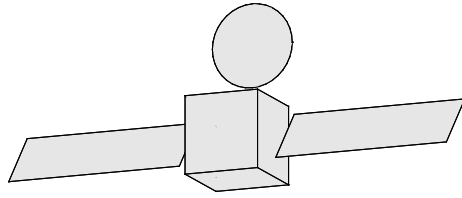


Figure 10. Box-Wing Shape Model

B. Angles and Light Curve Observations

With the addition of light curve observations, it should be possible to estimate the attitude state. It is desired to perform an analysis that determines when it is appropriate to bring in light curve data for estimation of additional object parameters. First, an object with a “box-wing” shape typical of GEO spacecraft is simulated with a fast spin (or “tumble”). This model is shown in Figure 10. It is assumed that m_{app} has zero-mean Gaussian noise with $\sigma = 0.1$ added. Attitude, angular rate, and orbit are estimated. It is seen that in this case, the singular values of the information matrix have contributions from both the attitude and orbit states. However, the singular values each are composed of contributions from primarily the orbit state or primarily the attitude state. This can be determined by looking at the right-hand side vectors of the singular value decomposition and by comparison to the singular values of the information matrix for orbit-only estimation. This phenomenon can be explained by the relatively small impact that the attitude states have on the orbital dynamics, compared to the orbital states, and vice-versa. For the attitude estimation filter to converge, significant *a priori* information is required, which is implemented through upper bounds on the initial covariance matrix. These have been found to be approximately 15 degrees in the rotation states and 25 degrees per hour in the angular rate state. If the initial covariance is too large, the filter typically

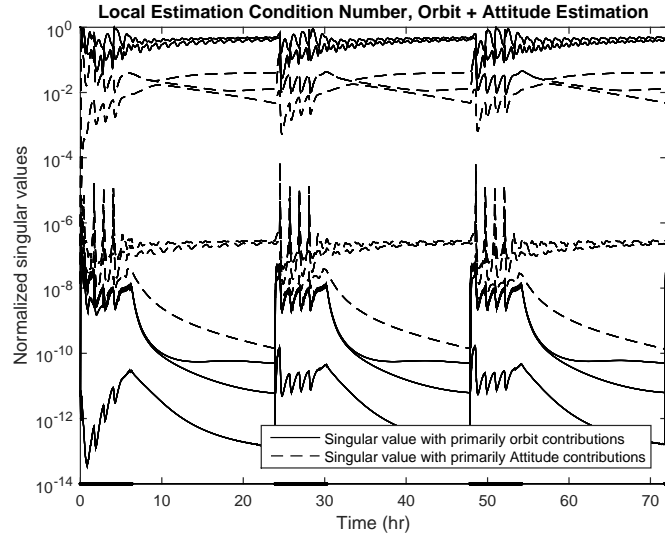


Figure 11. Normalized Singular Values of Information Matrix Showing Attitude Observability for GEO object. Solid black line on x -axis indicates measurements available.

diverges. Due to the relationship between information and observability, such a filter inherently requires an *a priori* observability. Nevertheless, the observability analysis is conducted in the same manner as before.

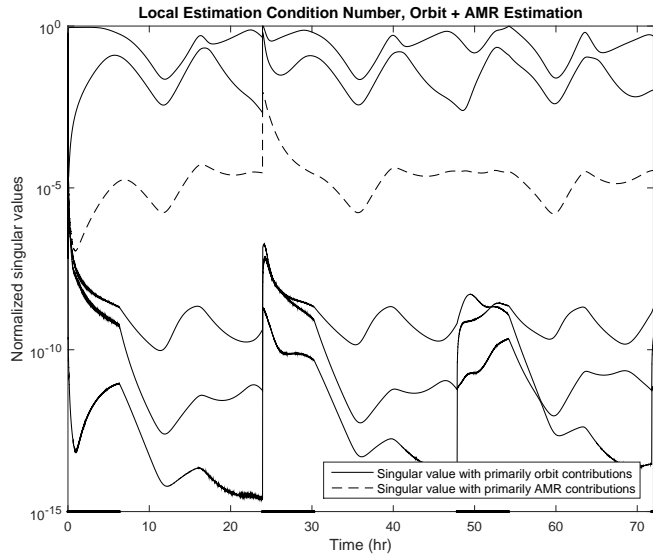


Figure 12. Normalized Singular Values of Information Matrix Showing AMR for GEO Object.

Figure 11 shows the local estimation condition number of the attitude and orbit filter. It is seen that there are three normalized singular values that have high observability - with a magnitude of approximately 10^{-2} . These are found to correspond to the angular velocity states – thus, these states are determined to have high observability. The three states with poor observability, with magnitudes around 10^{-7} or less, are found to correspond to the orientation states.

Figure 12 shows the local estimation condition numbers for the orbit and AMR filter for the same data. The normalized singular value with contributions from primarily AMR is identified, and it is seen that it has a magnitude of approximately 10^{-5} , as seen in the angles-only case. Despite the presence of additional information from the light curve, AMR still has better observability than the actual attitude state. This

occurs even though the AMR is not constant, but changes based on the attitude, and these changes must be accounted for through process noise covariance in the AMR state. Figure 13 shows this increased observability results in a better estimate, as the filter which estimates orbit and AMR is found to have a lower uncertainty.

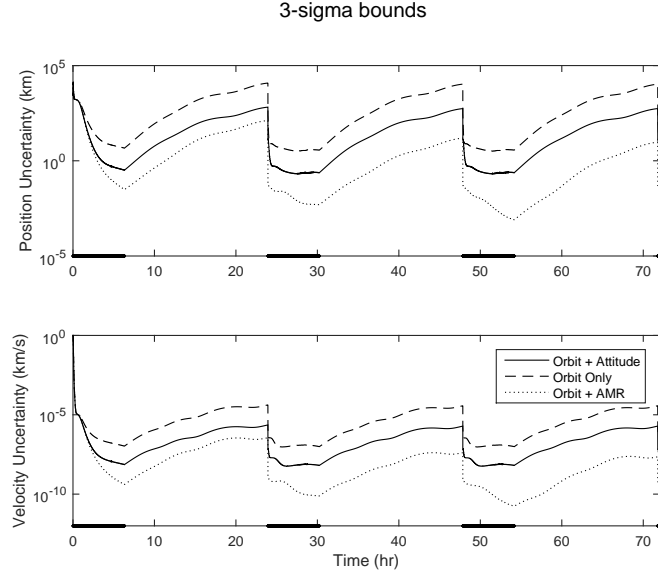


Figure 13. Uncertainty in Orbit States for Three Choices of Filter States.

C. Cannonball-to-Faceted Transition

The prior section has demonstrated a case where attitude estimation is not well-suited. A case of a spin-stabilized GEO satellite (with a slow spin rate) is now simulated. This slow spin rate means that A/m is not well-represented as a constant over a long time span, and as such, attitude estimation may improve the orbit estimates. The adaptive filter presented in section IV.D is implemented for this case, assuming the box-wing shape of Figure 10. The 3σ position uncertainty bounds are shown for the cannonball and adaptive filters in Figure 14. When switched on, it is seen that the adaptive estimator outperforms the cannonball model.

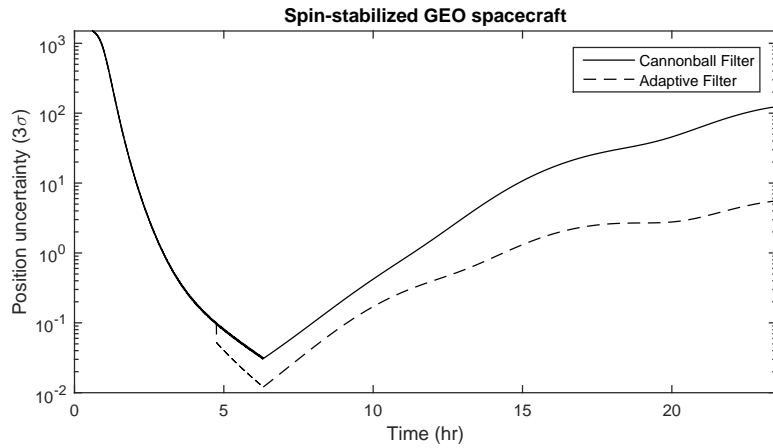


Figure 14. Position Uncertainties in Cannonball and Adaptive filters

Figure 15 shows the area-to-mass ratio estimate as well as the corresponding 3σ bounds for this object.

It is seen that the A/m estimate steadies out between 4 and 5 hours, and that the rate of decay of the covariance bounds slows. This is used to trigger the check for attitude observability. Figure 16 shows the

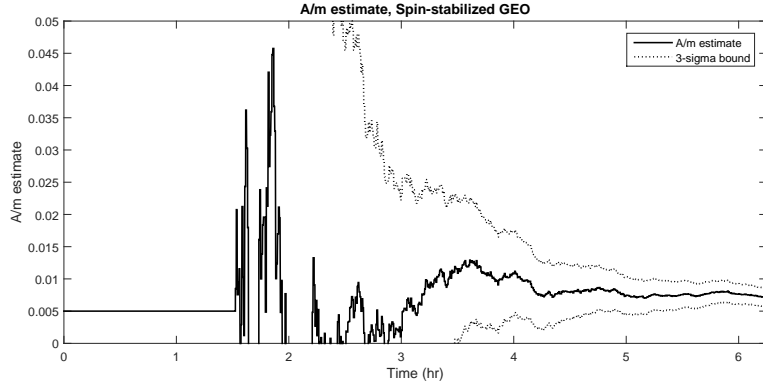


Figure 15. Area-to-Mass Ratio Estimate and 3σ Bounds

mutual information contributed by each measurement, propagating backward from the trigger point to the beginning of the track, for the cases of angles and angles + light curve observations. It is seen that the light curve produces a substantial increase in the amount of information when attitude is included in the state vector, indicating that attitude estimation may be possible. The filter is then begun from the beginning of the track as a MMAE filter, and at the trigger time, the weights immediately shift to favoring the faceted model, which is seen to provide a better estimate.

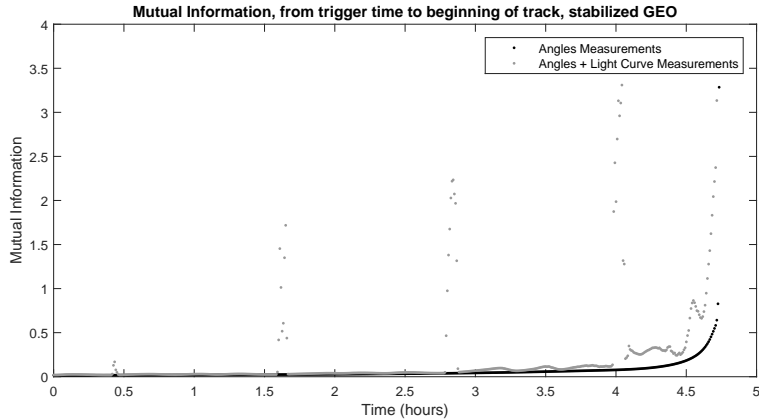


Figure 16. Mutual Information From Trigger Time Back to Beginning of Track, Box-Wing Object

The same filter is applied to a simulated sphere in the same orbit. As shown in Figure 17, the adaptive filter does not switch to a faceted model, and continues to follow the cannonball model. Figure 18 shows the mutual information with the attitude included in the state vector. It is seen that the addition of light curve data does not increase the mutual information, so attitude estimation is not attempted.

VI. Future Work

The utilization of observability for enabling improved conjunction assessment will be investigated. It is seen that the observability of orbital states and object characteristics directly affects the uncertainty in the estimate of the orbital states, and decreases in this uncertainty allow for better assessment of collision probability. Thus, the observability of the system will be directly applicable to conjunction assessment.

The application of observability to drive sensor scheduling will also be investigated. Each new observation adds information to the system, and thus increases the observability. However, this increase in the observability is not independent of the time between measurements, nor the position of the object and observer.

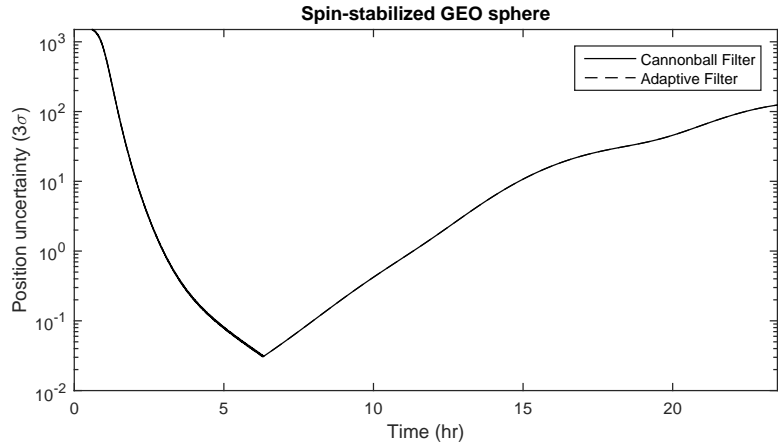


Figure 17. Position Uncertainties in Cannonball and Adaptive Filters for Spherical Object

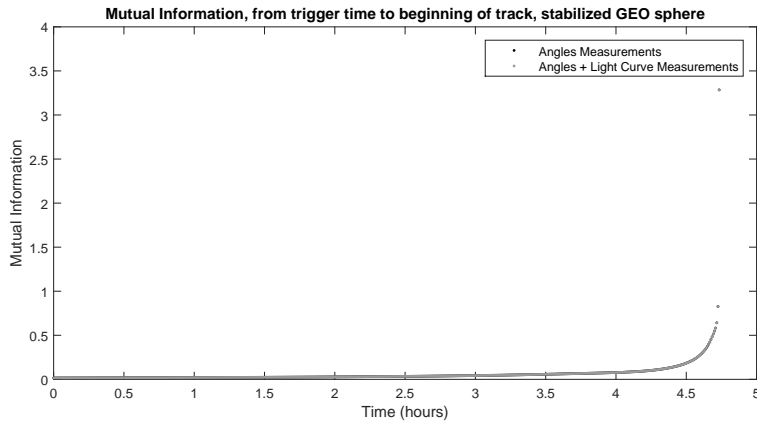


Figure 18. Mutual Information From Trigger Time Back to Beginning of Track, Spherical Object

Since sensor resources are limited, the use of observability to determine when it is necessary to take new observations to maintain a desired level of uncertainty will be investigated.

VII. Conclusion

It is seen that the uncertainty in state estimates is driven by the observability of the states used in the filter. The analysis showed that with the consider filter driven by the observability metric analysis, observation information was able to be more appropriately applied to a variety of objects and orbit regimes and provided insight into how successive night follow-up information can be utilized for improved object characterization. The importance of this successive night follow up is seen through the substantial increase in observability of the area-to-mass ratio parameter when these observations are added, even if measurements are taken frequently the previous night. This filtering process was then extended to the case where different choices of filter states are not independent, through the use of both observability analysis and Multiple Model Adaptive Estimation. The analysis provides an online assessment of the available information and shows the analyst the contribution of the observation types to the state estimation solution and can give insight into what future observations can provide in terms of state uncertainty reduction. The analysis shows that the observability of the system and system parameters can be used to trigger when it is appropriate to estimate additional states, and determine which parameters are the most appropriate to estimate.

Acknowledgments

The first author would like to thank the support of the Air Force Research Laboratory Research Space Scholars Program sponsored by the Universities Space Research Association.

References

- ¹Liu, J., "NORAD Satellite Tracking," *NASA Marshall Space Flight Center Upper and Middle Atmospheric Density Modeling Requirements for Spacecraft Design and Operations*, NASA, Huntsville, AL, Feb. 1987, pp. 89–94.
- ²McMahon, J. and Scheeres, D., "Space Object Catalog Maintenance Through Advances in Solar Radiation Pressure Modeling," *Journal of Guidance, Control, and Dynamics*, Vol. 38, No. 8, Aug. 2015, pp. 1366–1381, doi:10.2514/1.G000666.
- ³Hinks, J., Linares, R., and Crassidis, J., "Attitude Observability from Light Curve Measurements," *AIAA Guidance, Navigation, and Control Conference*, AIAA, Reston, VA, Aug. 2013, doi:10.2514/6.2013-5005.
- ⁴Linares, R., Jah, M. K., Crassidis, J. L., and Nebelecky, C. K., "Space Object Shape Characterization and Tracking Using Light Curve and Angles Data," *Journal of Guidance, Control, and Dynamics*, Vol. 37, No. 1, Jan.-Feb. 2014, pp. 13–25, doi:10.2514/1.62986.
- ⁵Wetterer, C. J. and Jah, M., "Attitude Estimation from Light Curves," *Journal of Guidance, Control and Dynamics*, Vol. 32, No. 5, Sept.–Oct. 2009, pp. 1648–1651, doi:10.2514/1.44254.
- ⁶Wetterer, C. J., Hunt, B., Hamada, C., Crassidis, J. L., and Kervin, P., "Shape, Surface Parameter, and Attitude Profile Estimation Using a Multiple Hypothesis Unscented Kalman Filter," *AAS/AIAA Space Flight Mechanics Meeting*, AAS, Springfield, VA, Jan. 2014, AAS Paper #14-303.
- ⁷Wetterer, C. J., Chow, C. C., Crassidis, J. L., and Linares, R., "Simultaneous Position Velocity, Attitude, Angular Rates, and Surface Parameter Estimation Using Astrometric and Photometric Observations," *16th International Conference on Information Fusion*, IEEE, Piscataway, NJ, July 2013, pp. 997–1004, doi:10.2514/6.2013-5005.
- ⁸Rapoport, I. and Bar-Itzhack, I., "On The Information Dilution Theorem and Its Application to Attitude Determination," *Journal of the Astronautical Sciences*, Vol. 49, No. 3, July–Sept. 2001, pp. 489–508.
- ⁹Dianetti, A., Weisman, R., and Crassidis, J., "Observability Analysis for Improved Space Object Characterization," *Journal of Guidance, Control, and Dynamics*, Submitted for Publication.
- ¹⁰Walker, M., Ireland, B., and Owens, J., "A Set of Modified Equinoctial Orbital Elements," *Celestial Mechanics*, Vol. 36, Aug. 1985, pp. 409–419.
- ¹¹Vallado, D. and McClain, W., *Fundamentals of Astrodynamics and Applications*, chap. 1, McGraw-Hill, New York, NY, 2nd ed., 2001, pp. 1–40.
- ¹²Wetterer, C. J., Linares, R., Crassidis, J. L., Kelecy, T. M., Ziebart, M. K., Jah, M. K., and Cefola, P. J., "Refining Space Object Radiation Pressure Modeling with Bidirectional Reflectance Distributions Functions," *Journal of Guidance, Control, and Dynamics*, Vol. 37, No. 1, Jan.–Feb. 2014, pp. 185–196, doi:10.2514/1.60577.
- ¹³Crassidis, J., Markley, F., and Cheng, Y., "Survey of Nonlinear Attitude Estimation Methods," *Journal of Guidance, Control, and Dynamics*, Vol. 30, No. 1, Jan.–Feb. 2007, pp. 12–28, doi:10.2514/1.22452.
- ¹⁴Ashikmin, M. and Shirley, P., "An Anisotropic Phong Light Reflection Model," Tech. rep., University of Utah, Salt Lake City, UT, 2000.
- ¹⁵Jazwinski, A., *Stochastic Processes and Filtering Theory*, chap. 7, Academic Press, San Diego, CA, 1970, pp. 231–234.
- ¹⁶Ristic, B., Arulampalam, S., and Gordon, N., *Beyond the Kalman Filter*, Artech House, Boston, MA, 2004, pp. 67–82.
- ¹⁷Krener, A. and Ide, K., "Measures of Unobservability," *Joint 48th IEEE Conference on Decision and Control and 28th Chinese Control Conference*, IEEE, Piscataway, NJ, 2009, doi:10.1109/CDC.2009.5400067.
- ¹⁸Papoulis, A. and Pillai, S., *Probability, Random Variables and Stochastic Processes*, McGraw Hill, New York, NY, 4th ed., 2002.
- ¹⁹Hermann, R. and Krener, A., "Nonlinear Controllability and Observability," *IEEE Transactions on Automatic Control*, Vol. AC-22, No. 5, October 1977, pp. 728–740.
- ²⁰Crassidis, J. and Junkins, J., *Optimal Estimation of Dynamic Systems*, chap. 4, Chapman & Hall/CRC, Boca Raton, FL, 2nd ed., 2012.
- ²¹Stauch, J. and Jah, M., "Unscented Schmidt-Kalman Filter Algorithm," *Journal of Guidance, Control, and Dynamics*, Vol. 38, No. 1, 2015, pp. 117–123, doi:10.2514/1.G000467.
- ²²Shuster, M., "A Survey of Attitude Representations," *Journal of the Astronautical Sciences*, Vol. 41, No. 4, Oct.–Dec. 1993, pp. 439–517.
- ²³Schaub, H. and Junkins, J., "Stereographic Orientation Paramters for Attitude Dynamics: A Generalization of the Rodrigues Paramters," *Journal of the Astronautical Sciences*, Vol. 4, No. 1, Jan.–March 1996, pp. 1–20.
- ²⁴Crassidis, J. and Markley, F., "Unscented Filtering for Spacecraft Attitude Estimation," *Journal of Guidance, Control, and Dynamics*, Vol. 26, No. 4, July-Aug. 2003, pp. 536–542, doi:10.2514/2.5102.